

Chain aggregation in dilute solutions of poly(methyl methacrylate) below the phase-separation temperature

Tomohide Nakagawa, Yoshiki Nakamura, Naoki Sasaki, and Mitsuo Nakata

Department of Polymer Science, Faculty of Science, Hokkaido University, Kita-ku, Sapporo 060-0810, Japan

(Received 26 May 2000; published 26 February 2001)

For dilute solutions of poly(methyl methacrylate) in isoamyl acetate with the molecular weight $M_w = 4.4 \times 10^6$, the phase-separation process was studied by static light-scattering measurements. The dilute solutions in the concentration range from 1.4×10^{-4} to 3.8×10^{-4} g/cm³ were quenched to about 16 K below the phase-separation temperature, and the aggregation processes of polymer chains were measured over a period of several hours. By analyzing the light-scattering data with the Guinier plot, the weight-averaged molecular weight $\langle M \rangle_w$ and z -averaged square radius $\langle R^2 \rangle_z^{1/2}$ for clusters of polymer chains were determined as a function of time t (min) and concentration c (g/cm³). The growth of clusters was represented by the exponential forms $\langle M \rangle_w / M(0) = e^{gct}$ and $\langle R^2 \rangle_z / R^2(0) = e^{hct}$ as a function of ct , where $M(0)$ and $R^2(0)$ were the values at $t=0$, and the constants g and h were determined to be $g = 11.6$ and $h = 7.5$. A double-logarithmic plot of $\langle M \rangle_w$ versus $\langle R^2 \rangle_z^{1/2}$ yielded a straight line with the slope $D = 3.06 \pm 0.02$. These characteristic features of the chain aggregation process were compared with the Smoluchowski equation for cluster-cluster aggregation with the collision kernel $(i+j)$ for i -mer and j -mer. The observed slow growth of clusters was attributed to the reaction-limited cluster aggregation. The chain density in a cluster was found to increase with an increase of the cluster size, resulting in the slope D exceeding 3.

DOI: 10.1103/PhysRevE.63.031803

PACS number(s): 61.25.Hq, 36.20.Ey

I. INTRODUCTION

For dilute solutions of poly(methyl methacrylate) (PMMA) in isoamyl acetate, phase separation occurs very slowly even far below the phase-separation temperature. Taking advantage of this nature of the solution, we studied the phase-separation process for the molecular weight $M_w = 2.35 \times 10^6$ and coil-globule transition for $M_w \times 10^{-6} = 2.35, 4.4, 8.4,$ and 12.2 by static light scattering measurements [1–3]. For solutions in the concentration range from 10^{-5} to 10^{-4} g/cm³, the coil-globule transition and the phase-separation process were observed separately for experimentally suitable time periods. The light-scattering measurements were carried out 30 min after setting a solution cell in a photometer on account of the thermal equilibration in the solution cell. This blank time in the initial stage did not seriously affect our experimental measurements because of the suitable ranges of the molecular weight and concentration.

Since for $M_w = 2.35 \times 10^6$ the polymer chain contracted to the equilibrium size in the first 30 min after quench, the kinetics of the chain collapse could not be observed but the process of the phase separation was measured [3]. For $M_w \times 10^{-6} = 8.4$ and 12.2 the process of the chain collapse was observed in a time period from several hundred minutes to a few thousand minutes in the globule temperature region [2]. Scattered intensities obtained during the process yielded the molecular weights correctly, which indicated that the effect of phase separation was negligible. For these molecular weights the phase separation process may be observed for an appropriate time period at higher concentrations, but consequently the chain collapse and the phase separation will occur competitively. For $M_w = 4.4 \times 10^6$ the polymer chain contracted to an equilibrium size in the first 30 min after

quench at higher temperatures but did not completely collapse during the time at lower temperatures in the globule region [2].

In the study of the phase-separation process for $M_w = 2.35 \times 10^6$, light-scattering data were analyzed by the Guinier plot to determine the average molecular weight $\langle M \rangle_w$ and radius $\langle R^2 \rangle_z^{1/2}$ of clusters of polymer chains [4]. The observed phase-separation process was expressed by the exponential growth of $\langle M \rangle_w \sim e^{Gt}$ and $\langle R^2 \rangle_z \sim e^{Ht}$, where the coefficients G and H were proportional to the concentration. This behavior was in agreement with the Smoluchowski equation [5] with the collision kernel $i+j$ for i -mer and j -mer [6,7]. Since the observed cluster formation process of polymer chains was very different from the phase-separation process in dilute polymer solutions [8,9], our experimental results were compared with the aggregation processes of colloidal particles [10]. This comparison and analysis by the Smoluchowski equation indicated that the exponential growth was due to a reaction-limited cluster aggregation (RLCA) rather than a diffusion-limited cluster aggregation (DLCA) [10–15].

The double-logarithmic plot of $\langle R^2 \rangle_z^{1/2}$ versus $\langle M \rangle_w$ obtained for $M_w = 2.35 \times 10^6$ was represented by a straight line with the slope $D = 2.86$ [3]. The considerable deviation from $D = 3$ was attributed to the cluster-size distribution rather than the cluster structure. The polymer-segment density of a cluster was assumed to be independent of the cluster size and was estimated to be roughly three times that of a single chain at the same temperature. The experimental value of $\ln \langle M \rangle_w$ ranged from 15 to 19, corresponding to the average number of chains in a cluster from 1.4 to 76. It is conceivable that the structure of a small-size cluster made of a few chains may be different from that of a large-size cluster. Our previous experiments were not suitable for revealing the properties of a

small-size cluster, because the cluster was not large enough for precise light scattering measurements and the observed values of $\langle M \rangle_w$ and $\langle R^2 \rangle_z$ deviated from the exponential growth at small times and at small concentrations. It is interesting to investigate the time evolution of the structure of cluster and to elucidate the slope D for the plot of $\langle R^2 \rangle_z^{1/2}$ versus $\langle M \rangle_w$.

In this study, we carried out light-scattering measurements on dilute solutions of PMMA with $M_w = 4.4 \times 10^6$ in isoamyl acetate at 30.0 °C. As predicted from the experimental results in the previous study [1,2], the PMMA chain collapsed to an equilibrium globule in the first 30 min after quench to 30.0 °C. The light-scattering measurements for the phase separation process revealed exponential growth of $\langle M \rangle_w$ and $\langle R^2 \rangle_z$ of clusters of polymer chains. According to an analysis based on the Smoluchowski equation, the polymer-segment density of a cluster increased with an increase of cluster size by a power law and approached a constant value for large clusters. The slope D was measured to be 3.06 ± 0.02 and was found to be attributed to the size distribution of clusters and the size dependence of the segment density of a cluster.

II. EXPERIMENT AND DATA ANALYSIS

As a PMMA sample, we used the same fraction $F13$ in the series $M19$ as was used in the previous study [1]. The sample has the molecular weight $M_w = 4.4 \times 10^6$ and the characteristic ratio $\langle s^2 \rangle_{oz} / M_w = 6.1 \times 10^{-18} \text{ cm}^2$, which gives a measure for the molecular weight distribution as $M_w / M_n = 1.17$ [2]. Isoamyl acetate was fractionally distilled immediately before use. The refractive index increment dn/dc for the present system has been obtained as a function of temperature, and $dn/dc = 0.0944$ was used at 30 °C [1].

Light scattering measurements were carried out at angular intervals of 15° in the range from 30° to 150° with unpolarized incident light at 435.8 nm. The photometer was calibrated with benzene as in the case of experiments for dilute polymer solutions, taking its Rayleigh ratio as $46.5 \times 10^{-6} \text{ cm}^{-1}$ at 25 °C [16]. Four solutions at concentrations $c(10^{-4} \text{ g/cm}^3) = 1.414, 2.324, 3.034, \text{ and } 3.787$ at 30.0 °C were prepared in each optical cell of 18 mm inner diameter. The solutions were filtered twice through a Sartorius membrane (SM 116, 0.8 μm) for optical clarification and stored in the dark near the θ temperature under saturated vapor of isoamyl acetate. A cylindrical cell located at the center of the photometer was filled with the solvent and kept at 30.0 °C by circulating thermostatted water to the jacket. The optical cell was immersed in the cylindrical cell, and scattered intensities were measured at time intervals of about 30 min after the quench. During the measurements the solutions were transparent to the eye and the multiple scattering effect was negligibly small.

To determine the phase-separation temperature, the solution was quenched to low temperatures. At each temperature scattered intensity from the solution was monitored for a few days because of a long incubation time. The temperature at which scattered intensity began to increase was taken as the phase-separation temperature T_p . Since the lag period was

extraordinarily long near T_p and at low concentrations, the quench temperature was changed at every 0.5 K. Thus, T_p was determined to be 45.0, 46.0, 47.0, and 47.5 °C at $c(10^{-4} \text{ g/cm}^3) = 1.414, 2.324, 3.034, \text{ and } 3.787$, respectively.

For dilute polymer solutions, light scattering data at an angle θ are analyzed with the excess Rayleigh ratio R_θ from polymers. By neglecting the terms due to the virial coefficient, R_θ can be related to the molecular weight m and the scattering function $P(q)$ for a polymer chain by [17]

$$R_\theta / Kc = mP(q), \quad (1)$$

where K and the argument q are defined as $K = (2\pi^2 n^2 / N_A \lambda^4) (dn/dc)^2$ and $q = (4\pi n / \lambda) \sin(\theta/2)$, respectively. Here, N_A is Avogadro's number, n is the refractive index of the solution, and λ is the wavelength of the incident light in a vacuum. Hence, we use m for the molecular weight of a polymer and M for the molecular weight of a cluster of polymers.

In the aggregation process of polymer chains, the optical constant K and the concentration c in Eq. (1) remain unchanged, but c is given by the sum of c_k , $\sum c_k$ for various k -mers including monomer $k=1$ (single polymer chain). Accordingly, the Rayleigh ratio R_θ from the clusters is given by the sum $\sum Kc_k M_k P_k(q)$ for k -mers with the molecular weight $M_k (= km)$ and scattering function $P_k(q)$. Thus, R_θ can be expressed as

$$R_\theta = Kc \langle M \rangle_w \langle P(q) \rangle_z. \quad (2)$$

with

$$\langle M \rangle_w = \frac{\sum M_k c_k}{\sum c_k} \quad (3)$$

and

$$\langle P(q) \rangle_z = \frac{\sum P_k(q) M_k c_k}{\sum M_k c_k}. \quad (4)$$

Here, $\langle M \rangle_w$ and $\langle P(q) \rangle_z$ are the weight-averaged molecular weight and the z -averaged scattering function for clusters. For spherical particles, Eq. (2) can be expressed by the approximate form [4]

$$\ln(R_\theta / Kc) = \ln \langle M \rangle_w - \frac{1}{5} \langle R^2 \rangle_z q^2, \quad (5)$$

where $\langle R^2 \rangle_z$ is the z -averaged square radius. According to Eq. (5), light scattering data were analyzed by the Guinier plot to determine $\langle M \rangle_w$ and $\langle R^2 \rangle_z$ of the clusters.

III. EXPERIMENTAL RESULTS

Figure 1 shows the Guinier plot for scattered intensities from the solution at $c = 2.324 \times 10^{-4} \text{ g/cm}^3$. The plots from the bottom were obtained at 30, 210, 390, 540, 720, 900, 1080, and 1290 min after quench to 30.0 °C, respectively. The solid lines were given to show the behavior of data points. On the basis of Eq. (5), $\langle M \rangle_w$ (g/mol) and $\langle R^2 \rangle_z$ (nm²) at each time were evaluated from the intercept and the initial slope of the line, respectively. At other con-

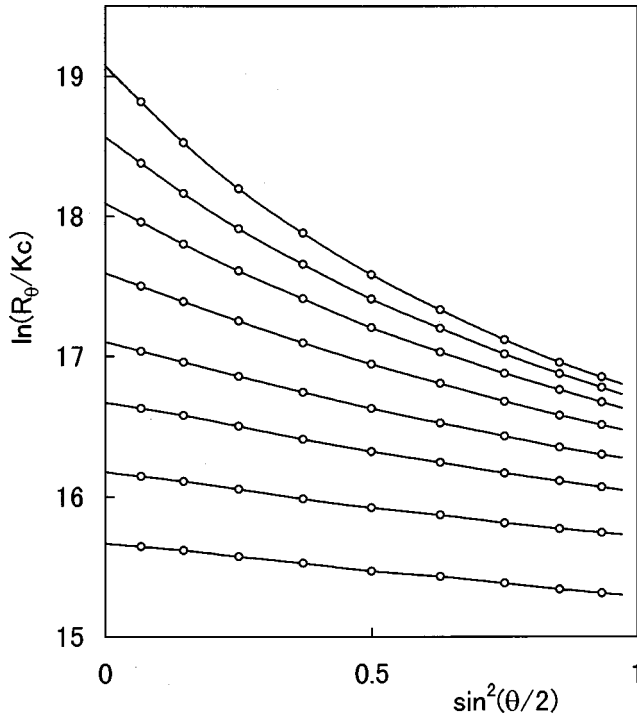


FIG. 1. Guinier plots for scattered intensities from PMMA in isoamyl acetate at $c = 2.324 \times 10^{-4} \text{ g/cm}^3$ according to Eq. (5) with R_g/K_c (g/mol). Curves from bottom to top were obtained at 30, 210, 390, 540, 720, 900, 1080, and 1290 min after quench to 30.0 °C.

centrations, light scattering data were analyzed in the same manner to determine $\langle M \rangle_w$ and $\langle R^2 \rangle_z$ at each time. Figure 2 shows a plot of $\ln \langle M \rangle_w$ versus the time t (min) for solutions at $c(10^{-4} \text{ g/cm}^3) = 1.414$ (○), 2.324 (△), 3.034 (□), and 3.787 (×). Figure 3 shows a plot of $\ln \langle R^2 \rangle_z$ versus t (min) with the same symbols as those used in Fig. 2. The plots in Figs. 2 and 3 are represented by straight lines and can be fitted to the relations

$$\ln \langle M \rangle_w = \ln M(0) + Gt. \quad (6)$$

$$\ln \langle R^2 \rangle_z = \ln R^2(0) + Ht. \quad (7)$$

where $M(0)$ and $R^2(0)$ are the values extrapolated to $t=0$. Table I gives the values of $M(0)$, $R^2(0)$, G , and H estimated from the straight lines in Figs. 2 and 3. Figure 4 shows the plots of G and H against c . Each plot yields a straight line passing through the origin. The slopes of the plots of G and H versus c were estimated to be $11.4 \text{ cm}^3 \text{ g}^{-1} \text{ min}^{-1}$ and 7.3, respectively. Thus, the plots of $\ln \langle M \rangle_w / M(0)$ and $\ln \langle R^2 \rangle_z / R^2(0)$ versus ct should be represented by single straight lines. Figure 5 shows the reduced plots for $\langle M \rangle_w$ and $\langle R^2 \rangle_z$ by open circles and triangles, respectively. As expected, each plot can be fitted to a straight line. Thus, the present data can be expressed by the following:

$$\langle M \rangle_w / M(0) = \exp(gct), \quad (8)$$

$$\langle R^2 \rangle_z / R^2(0) = \exp(hct), \quad (9)$$

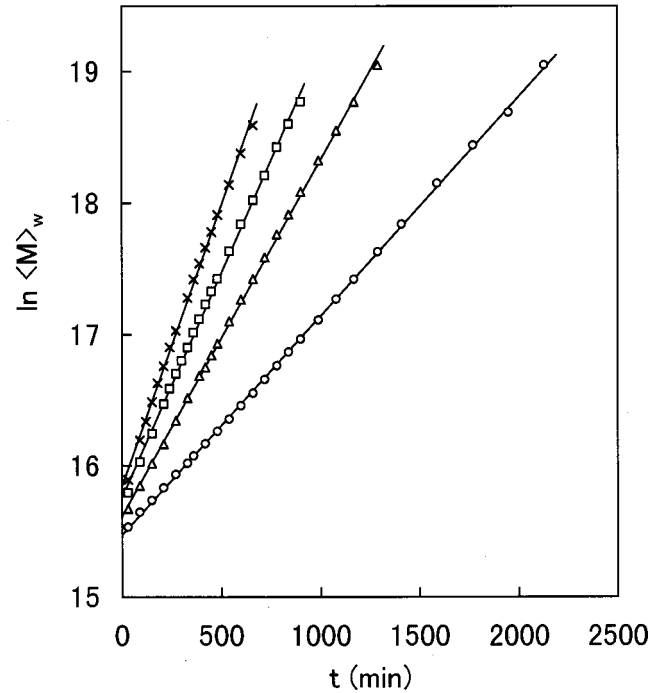


FIG. 2. Semilogarithmic plots of weight-averaged molecular weight $\langle M \rangle_w$ (g/mol) of clusters versus time t (min) at various concentrations. Data points were obtained at $c(10^{-4} \text{ g/cm}^3) = 1.414$ (○), 2.324 (△), 3.034 (□), and 3.787 (×).

where the coefficients g and h were determined as $g = 11.6 \text{ cm}^3 \text{ g}^{-1} \text{ min}^{-1}$ and $h = 7.5$ from the straight lines in Fig. 5. These values agree well with those estimated from the plots in Fig. 4.

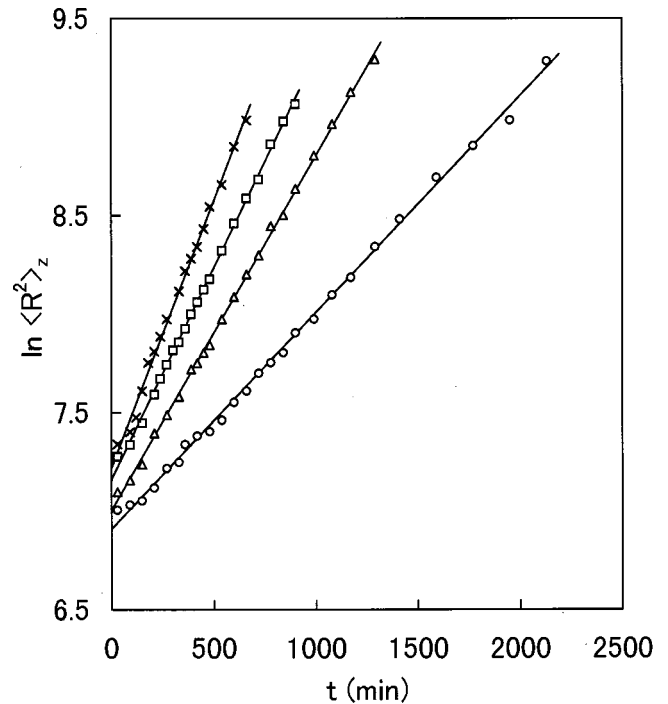


FIG. 3. Semilogarithmic plots of z -averaged square radius $\langle R^2 \rangle_z$ (nm²) of clusters versus time t (min) at various concentrations. Symbols of data points are the same as those in Fig. 2.

TABLE I. Concentration dependence of the parameters $M(0)$ and G in Eq. (6), and $R^2(0)$ and H in Eq. (7). The present data were obtained for the molecular weight $m=4.4\times 10^6$ and previous data for $m=2.35\times 10^6$ (Ref. [3]).

c (10^{-4} g/cm 3)	$M(0)$ (10^6 g/mol)	G (10^{-3} min $^{-1}$)	$R^2(0)$ (10^3 nm 2)	H (10^{-3} min $^{-1}$)	$R(0)M^{1/3}(0)$ (nm mol $^{1/3}$ /g $^{1/3}$)
$m=4.4\times 10^6$					
1.414	5.24	1.67	1.002	1.10	0.182
2.324	6.06	2.71	1.097	1.80	0.182
3.034	6.98	3.42	1.287	2.15	0.188
3.787	7.59	4.28	1.366	2.71	0.188
$m=2.35\times 10^6$					
1.30	1.28	6.86	0.347	4.91	0.172
2.66	2.33	13.9	0.572	9.53	0.180
4.04	3.51	20.8	0.721	14.6	0.177
5.37	4.20	28.8	0.854	18.7	0.181

Figure 6 shows the plot of $\ln\langle M \rangle_w$ versus $\ln\langle R^2 \rangle_z^{1/2}$ for the data at the four concentrations. The data points given by open circles construct a single straight line independent of time and concentration. Thus, the relation between $\langle M \rangle_w$ and $\langle R^2 \rangle_z$ can be expressed by the power law as

$$\langle R^2 \rangle_z^{1/2} = A_p \langle M \rangle_w^{1/D}. \quad (10)$$

By a least-squares fit, the exponent D and the coefficient A_p were determined as $D=3.06\pm 0.02$ and $A_p=0.204\pm 0.005$. It is clear that the exponent D exceeds 3.

Figure 7 shows the semilogarithmic plot of $\langle P(x) \rangle_z$ ($=R_\theta/Kc\langle M \rangle_w$) versus $x^2=\langle R^2 \rangle_z q^2$, where $\langle P(x) \rangle_z$ was es-

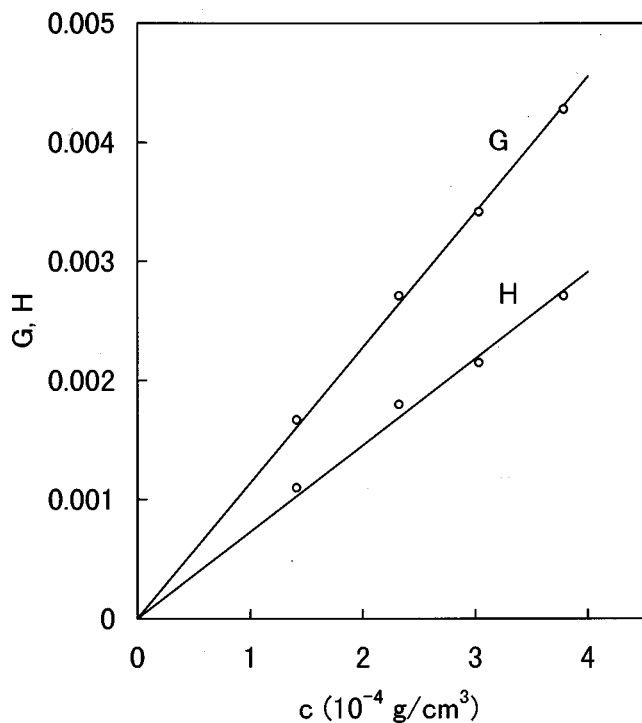


FIG. 4. Slope G for the plot of $\ln\langle M \rangle_w$ versus t and slope H for the plot of $\ln\langle R^2 \rangle_z$ versus t as a function of the concentration c .

timated for the solution at $c=2.324\times 10^{-4}$ g/cm 3 and at 720 (\circ), 900 (\triangle), 1080 (\square), and 1290 min (\times). The data points obtained at different times appear to construct a single composite line in the whole range of x^2 . The data points at the other concentrations were found to fall on the same line.

IV. COMPARISON WITH THE SMOLUCHOWSKI EQUATION

Smoluchowski formulated aggregation kinetics in terms of cluster-cluster collisions [5]. k -mers are formed by collisions of i -mers and j -mers ($k=i+j$) and grow into larger

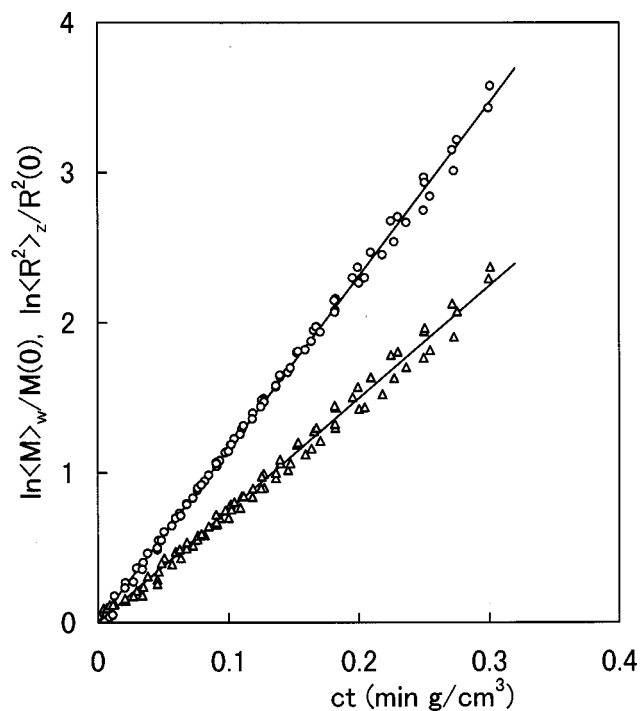


FIG. 5. Plots of $\ln\langle M \rangle_w/M(0)$ versus ct (open circles) and $\ln\langle R^2 \rangle_z/R^2(0)$ versus ct (triangles) for data at various values of time t (min) and concentration c (g/cm 3) for $m=4.4\times 10^6$. The former and latter plots yield the slope $g=11.6$ and $h=7.5$, respectively.

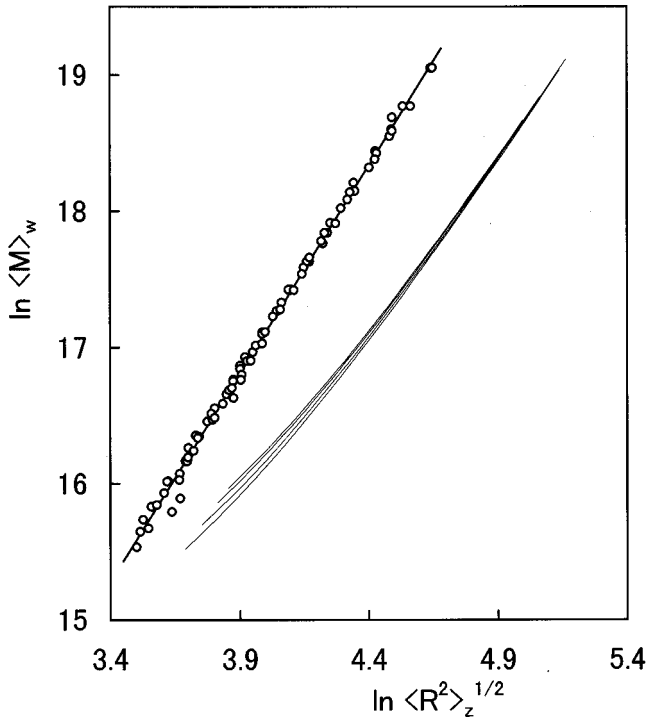


FIG. 6. Double-logarithmic plot of $\langle M \rangle_w$ versus $\langle R^2 \rangle_z^{1/2}$ for data at various times and concentrations. The straight line fitted to the data points gives the exponent $D = 3.06 \pm 0.02$. The four thin lines represent a double-logarithmic plot of $\langle M \rangle_w$ versus $(\langle M^{2/3} \rangle_z / 20)^{1/2}$ calculated with Eqs. (14) and (16) at the experimental concentrations. The factor 1/20 is for the convenience of the scale in abscissa.

clusters by collisions with other clusters. By assuming a random distribution of clusters in solution, the time evolution of the number $N_k(t)$ of k -mer ($k = 1, 2, \dots$) in unit volume was derived with the collision kernel K_{ij} in the form

$$dN_k/dt = (1/2) \sum_{i+j=k} K_{ij} N_i N_j - N_k \sum_j K_{kj} N_j. \quad (11)$$

Equation (11) has been solved only for $K_{ij} = 1$, $i + j$, ij and their linear combinations, while the moments of the distribution defined by $Q_n(t) = \sum_k k^n N_k(t)$ can be easily calculated by [6]

$$dQ_n/dt = (1/2) \sum_i \sum_j [(i+j)^n - i^n - j^n] K_{ij} N_i N_j. \quad (12)$$

The first moment Q_1 represents the total number N of monomers and should be constant. The number-averaged molecular weight and weight-averaged molecular weight of clusters are expressed as $\langle M \rangle_n = m Q_1(t) / Q_0$ and $\langle M \rangle_w = m Q_2(t) / Q_1$, respectively. For a given form of K_{ij} , an explicit expression of Q_n can be obtained for an initial condition. In the present experiment, the initial condition is given by $N_1(0) = N (= c/m)$ and $N_i(0) = 0 (i \geq 2)$. Thus, for $K_{ij} = B(i+j)$ with B as a constant, Eq. (12) gives $\langle M \rangle_n = m \exp(Bct/m)$ and

$$\langle M \rangle_w = m \exp(2Bct/m). \quad (13)$$

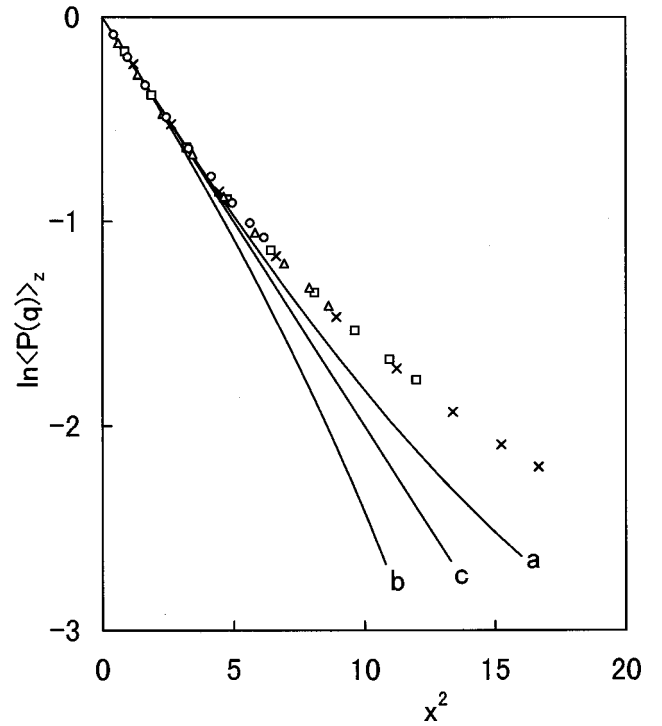


FIG. 7. Guinier plot of the scattering function $\langle P(q) \rangle_z$ against $x^2 = \langle R^2 \rangle_z q^2$. Data points were obtained at $c = 2.324 \times 10^{-4} \text{ g/cm}^3$ and at $t(\text{min}) = 720$ (\circ), 900 (\triangle), 1080 (\square), and 1290 (\times). The line a was calculated at the same values of c and t as the data points by using Eqs. (4), (17), (19), and (21). The line b is for monodisperse spheres. The straight line c has the initial slope of $1/3$ for spheres.

Equation (13) agrees with Eq. (8) in the functional form and in the scaled time ct , $M(0)$ in Eq. (8) depends on c due to the interaction between polymer chains and gives an apparent molecular weight, while the factor g can be equated to $2B/m$. Thus, we have $2B/m = 11.6$.

It is possible to evaluate the z -averaged square radius $\langle R^2 \rangle_z$ by using the Smoluchowski equation provided that the distribution $N_k(t)$ is given explicitly and the relation between the molecular weight $M_k (= km)$ and the radius R_k of k -mer is known. First, we assumed the relation

$$R_k = A(km)^{1/D}, \quad (14)$$

where A is a constant for a monodisperse cluster and may be different from A_p in Eq. (10) for a polydisperse cluster. D in Eq. (14) may be different from that in Eq. (10). By using Eq. (14), we have

$$\langle R^2 \rangle_z = A^2 \langle M^{2/D} \rangle_z, \quad (15)$$

with

$$\langle M^{2/D} \rangle_z = \frac{\sum (km)^{2/D} k^2 N_k}{\sum k^2 N_k}. \quad (16)$$

For the present initial condition, the solution of Eq. (11) with $K_{ij} = B(i+j)$ has been written explicitly as [6,7]

$$N_k(t) = N(1-b)e^{-kb}(kb)^{k-1}/k!, \quad (17)$$

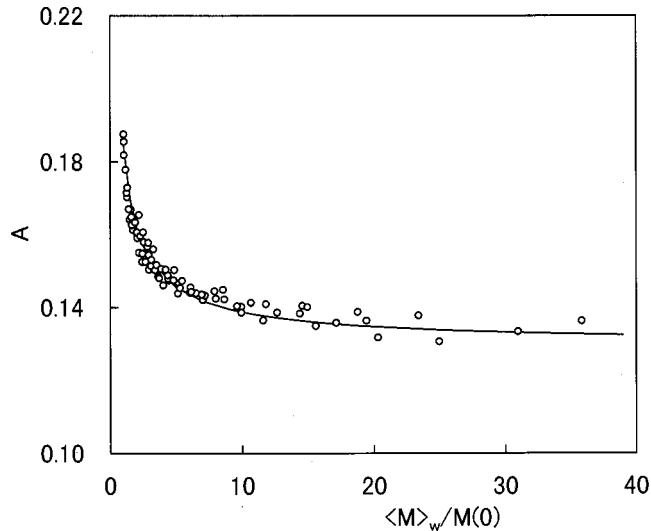


FIG. 8. Values of A in Eq. (14) as a function of observed $\langle M \rangle_w / M(0)$. A^2 was estimated as a ratio of $\langle R^2 \rangle_z$ observed to $\langle M^{2/3} \rangle_z$ calculated by Eq. (17) and $g = 11.6$. The solid line is described by Eq. (20) with $p = 0.124$ and $q = 0.42$.

with $b = 1 - e^{-(B/m)ct}$. It should be noted that $N_k(t)$ depends on time t through b with the scaled time ct . We assumed $D = 3$ in Eq. (14), because polymer chains for $M_w = 4.4 \times 10^6$ were in the globule state at 30.0°C [1]. Since the value of m [$=M(0)$] at each concentration has been estimated as shown in Table I, and $2B/m$ is given by $g = 11.6$, we can calculate $\langle M \rangle_w$ and $\langle M^{2/D} \rangle_z$ at each concentration and at each time corresponding to the experimental data. In Fig. 6, the plot of $\ln(\langle M^{2/D} \rangle_z / 20)^{1/2}$ versus $\ln \langle M \rangle_w$ due to the calculation is shown by thin lines, where the factor $\frac{1}{20}$ is for the convenience of scale in the abscissa. The plot shows marked curvature and noticeable dependence on the concentration at small $\ln \langle M \rangle_w$, while the plot appears to converge on a line with the slope 3.0 at large $\ln \langle M \rangle_w$. In fact, the slope of the plot was found to approach 3.0 near $\ln \langle M \rangle_w = 21$. The calculated curves are considerably different from the behavior of the experimental data points in slope and concentration dependence.

The coefficient A in Eq. (14) was evaluated as a ratio of the observed value of $\langle R^2 \rangle_z^{1/2}$ to the calculated value of $\langle M^{2/D} \rangle_z^{1/2}$ for $D = 3$. In Fig. 8, the estimated values of A ($\text{nm mol}^{1/3}/\text{g}^{1/3}$) are plotted against the observed values of $\langle M \rangle_w / M(0)$, which indicates the weight-average number of chains in a cluster. The data points at different concentrations appear to construct a single composite curve. In Table I, $R(0)/M(0)^{1/3}$ seems to be constant compared to the large dependence of $M(0)$ and $R^2(0)$ on c and yields an average value of 0.185. Thus, a composite curve for the data points should start from $A_1 = 0.185$ at $\langle M \rangle_w / M(0) = 1$ and may approach a constant value at large $\langle M \rangle_w / M(0)$. The relation between A and $\langle M \rangle_w / M(0)$ was found to be well represented by a power law as

$$A = u + (A_1 - u) \{ \langle M \rangle_w / M(0) \}^{-\nu}. \quad (18)$$

In fact, the values of $u = 0.129$ and $\nu = 0.76$ can reproduce

the behavior of A as shown by the solid line in Fig. 8. Thus, Eq. (18) asserts that A depends on the cluster size k , and Eq. (14) should be rewritten as

$$R_k = A_k (mk)^{1/D}, \quad (19)$$

with $D = 3$. The relation between A_k and k may have the form

$$A_k = p + (A_1 - p)k^{-q}, \quad (20)$$

with $A_1 = 0.185$. The constants p and q in Eq. (20) were determined in such a way that the calculated z -averaged square radius $\langle A^2 M^{2/D} \rangle_z$ may agree with the experimental value of $\langle R^2 \rangle_z$. We obtained an agreement between calculated $\langle A^2 M^{2/D} \rangle_z / A_1^2 M^{2/D}(0)$ and observed $\langle R^2 \rangle_z / R^2(0)$ within an error of 1% for $p = 0.124$ and $q = 0.42$. Naturally, these values of p and q can reproduce the observed exponent D in Eq. (10) as 3.09 ± 0.02 . Thus, the observed constant value of D can be explained by Eq. (20) for the size dependence of A_k and Eq. (17) for the size distribution and may not be attributed to a self-similar structure of the clusters.

Equation (20) implies that the segment density of a cluster increases with an increase of cluster size. Clusters of a few polymer chains may have a transient structure different from a sphere of a uniform density profile. However, under the assumption of a spherical cluster of uniform density, A_k gives a measure for packing of polymer chains in a cluster, because $A_k^3 = R_k^3 / M_k$ is proportional to the specific volume of a cluster.

We obtain $A_1 = 0.185 \text{ nm mol}^{1/3}/\text{g}^{1/3}$ and $A_1^3 = 0.0063$ for a single polymer chain, while we have $A_\infty = 0.124$ and $A_\infty^3 = 0.0019$ for a sufficiently large cluster. A_∞^3 for the large cluster is roughly one third of A_1^3 for a single chain: in a larger cluster, polymer chains undergo further contraction and/or penetrate one another. An alternative parameter to characterize the cluster is the polymer mass concentration $c_k = 3/(4\pi N_k A_k^3)$. From the above values of A_1 and A_∞ , we have $c_1 = 0.063 \text{ g/cm}^3$ and $c_\infty = 0.21$. The concentration for the single polymer at the θ -temperature is estimated to be 0.0075 g/cm^3 , which is much lower than c_1 and c_∞ .

The scattering function $\langle P(q) \rangle_z$ at each concentration and each time can be calculated by using Eqs. (4) and (17). It was assumed that the scattering function $P_k(q)$ for k -mer could be expressed by

$$P_k(q) = \{ [3/(R_k q)^3] [\sin(R_k q) - (R_k q) \cos(R_k q)] \}^2 \quad (21)$$

for spheres [4], where R_k is given by Eqs. (19) and (20). We calculated $\langle P(q) \rangle_z$ at the same values of c and t as those for the scattering data in Fig. 7. The four scattering functions calculated at different times closely agree with one another and yield the composite curve a . The line b is calculated for monodisperse spheres and the straight line c is given with the initial slope $1/5$ for spheres. At large x^2 the line a is much closer to the data points than lines b and c . The Guinier plot has been used to determine the size of monodisperse spherical particles because of a wide range of the initial slope. For polydisperse spherical particles, the range of the initial slope

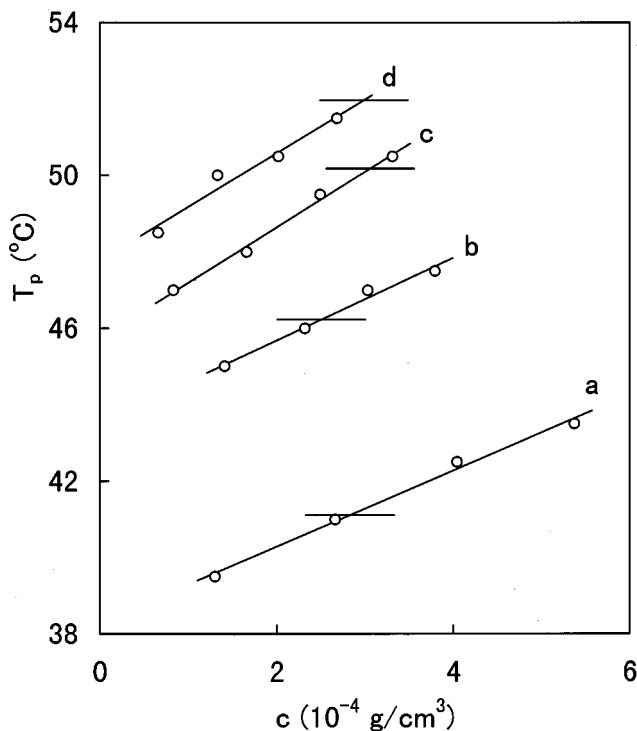


FIG. 9. Cloud-point curves of PMMA in isoamyl acetate for the molecular weight $m \times 10^{-6} = 2.35$ (curve a), 4.4 (curve b), 8.4 (curve c), and 12.2 (curve d). The short horizontal lines indicate coil-globule crossover temperature estimated by $(1 - \theta/T)m^{1/2} = -97$.

may depend on the form of the size distribution and is not known *a priori*. The curves *a* and *b* agree with the straight line *c* in the ranges of $x^2 < 5$ and $x^2 < 2$ within 3% error, respectively. A curve fitted to the experimental points agreed with the line *c* in $x^2 < 2.5$ within the same error. Thus, the Guinier plot can be used for the present system with the same reliability as in the case for monodisperse particles.

The present light scattering equations are based on the Rayleigh-Debye approximation, which may be valid for $4\pi \langle R^2 \rangle_z^{1/2} (m-1) / \lambda' \ll 1$, where m is the ratio of the refractive index of the cluster to that of the solvent and λ' is the wavelength of the light in the solution [18]. The largest size of clusters observed was $\langle R^2 \rangle_z^{1/2} = 104$ nm. $m-1$ was estimated roughly to be 0.014 with $dn/dc = 0.0944$, $c_\infty = 0.21$ g/cm³, and the refractive index of solvent 1.406. Then, $4\pi \langle R^2 \rangle_z^{1/2} (m-1) / \lambda'$ was estimated to be 0.06. Thus, the Rayleigh-Debye approach can be used for the present system. As expected from the above estimation, no depolarization was observed for the scattered light from polymer chain clusters.

V. DISCUSSION AND CONCLUSION

In usual liquid mixtures the rate of a phase separation depends strongly on the quench depth from the phase-separation temperature, i.e., cloud-point temperature. Figure 9 shows a plot of the observed cloud-point temperature T_p against the concentration c . The curve *b* was obtained for

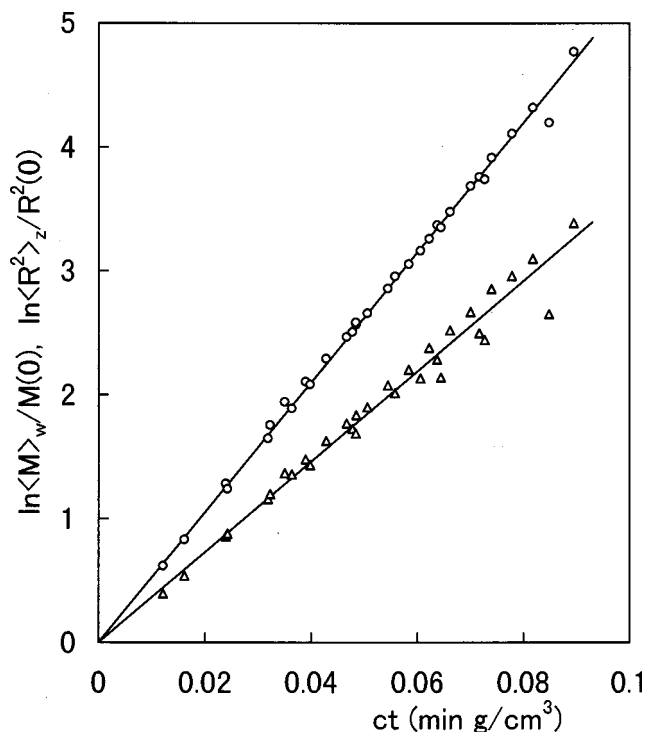


FIG. 10. Plots of $\ln \langle M \rangle_w / M(0)$ versus ct (open circles) and $\ln \langle R^2 \rangle_z / R^2(0)$ versus ct (triangles) for data at various values of time t (min) and concentration c (g/cm³) for $m = 2.35 \times 10^6$ (Ref. [3]). The former and latter plots give the slope $g = 52.4$ and $h = 36.5$, respectively.

$m \times 10^{-6} = 4.4$ in the present study, and the curves *a*, *c*, and *d* were obtained for $m \times 10^{-6} = 2.35$, 8.4, and 12.2 in the previous studies, respectively [2,3]. The cloud-point curve shifts to a higher temperature and has a larger slope with increasing molecular weight. The short horizontal line indicates the coil-globule crossover temperature calculated by $(1 - \theta/T)m^{1/2} = -97$ [1]. Each horizontal line intersects the cloud-point curve near $c = 3 \times 10^{-4}$ g/cm³. It is difficult to observe the influence of the chain collapse on the cloud-point curve. Because of the increase of T_p with increasing concentration, the plots in Figs. 4 and 5 are constructed with data points at different quench depths from the cloud-point temperature. However, the single composite lines in Fig. 5 indicate that the phase-separation process is dominated by the temperature distance $1 - \theta/T$ from the θ -temperature rather than by the quench depth from T_p .

In the previous study [3], the phase-separation process was investigated for $m = 2.35 \times 10^6$ at 25.0 °C. The plots of $\ln \langle M \rangle_w$ and $\ln \langle R^2 \rangle_z$ versus t yielded straight lines, and the constants in Eqs. (6) and (7) were determined as shown in Table I. Note that the slopes G and H were expressed by the small letters in the previous study. For the lowest concentration we determined the slope with data at later times because of the very slow cluster growth in the initial stage. However, the slopes G and H were proportional to c , and the scaled plots in the form of Eqs. (8) and (9) were predicted. Figure 10 shows the scaled plots for $\langle M \rangle_w$ (open circles) and $\langle R^2 \rangle_g$ (triangles), and the straight lines fitted to data points yield $g = 52.4$ and $h = 36.5$, which agree with the previous values.

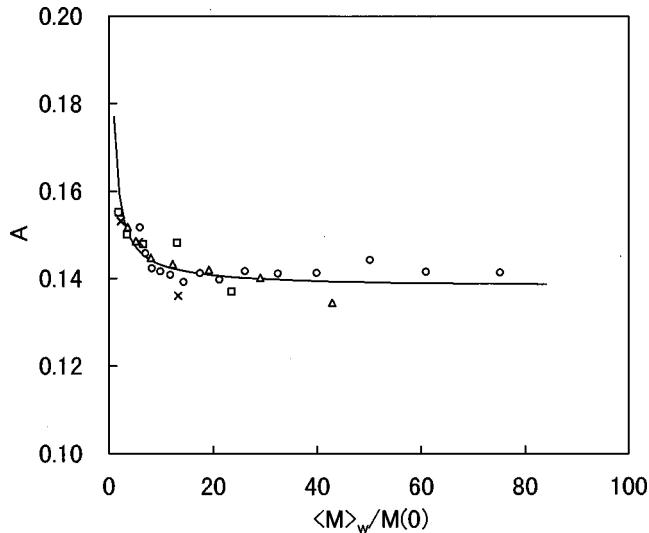


FIG. 11. Values of A in Eq. (14) as a function of observed $\langle M \rangle_w / M(0)$ for $m = 2.35 \times 10^6$ (Ref. [3]). A^2 was estimated as a ratio of $\langle R^2 \rangle_z$ observed to $\langle M^{2/3} \rangle_z$ calculated by Eq. (17) and $g = 52.4$. The solid line is given by Eq. (20) with $p = 0.138$ and $q = 0.71$. Data points were obtained at $c(10^{-4} \text{ g/cm}^3) = 1.30(\circ)$, 2.66 (Δ), 4.04 (\square), and 5.37 (\times).

In the plots data points at small t for lower concentrations are omitted because of the marked deviation from the straight lines. We reanalyzed the previous data with $g = 52.4$ and $h = 36.5$ by the same method as the present ones and obtained A in Eq. (14), A_k in Eq. (19) and $\langle P(q) \rangle_z$.

Figure 11 shows the plot of A versus $\langle M \rangle_w / M(0)$ for the same data points as those in Fig. 7 of Ref. [3]. At $ct = 0$, i.e., $\langle M \rangle_w / M(0) = 1$, A is equal to $R(0)/M(0)^{1/3}$ given in Table I. The values of $M(0)$ and $R(0)$ at the lowest concentration are very small because of the use of data points at later times (see Figs. 2 and 3 in Ref. [3]). Nevertheless, $R(0)/M^{1/3}(0)$ seems to be independent of c and gives the average value of 0.177. Correspondingly, the data points in Fig. 11 may be fitted to a single curve starting from $A_1 = 0.177$ at $\langle M \rangle_w / M(0) = 1$. The solid curve in Fig. 11 is described by Eq. (18) with $u = 0.138$ and $v = 0.88$. In the previous study, we could not characterize the behavior of A because of a small number of data points at small ct and an inappropriate plot of A versus $\ln \langle M \rangle_w$. On account of the marked dependence of A on $\langle M \rangle_w / M(0)$, again we assumed Eq. (20) and determined p and q by comparing $\langle R^2 \rangle_z$ calculated with Eqs. (17), (19), and (20) with the observed one. The values of $\langle R^2 \rangle_z / R^2(0)$ calculated with $p = 0.138$ and $q = 0.71$ were found to agree with Eq. (9) with $h = 36.5$ within an error of 1%. These values of p and q reproduced the observed slope $D = 2.86$ in Eq. (10) correctly. The ratio $(A_1 / A_\infty)^3$ for the specific volume of a monomer to a sufficiently large cluster is estimated to be 2.1. The value of q indicates that A_k for $m = 2.35 \times 10^6$ approaches the asymptotic value p faster than A_k for $m = 4.4 \times 10^6$.

Although the introduction of the k dependence of A_k explained the behavior of $\langle R^2 \rangle_z$ reasonably, we can see a noticeable discrepancy between the data points and the calculated curve a at large x^2 in Fig. 7. For clusters of polymer

chains we used Eq. (21) for spheres of uniform density, because $\langle P(q) \rangle_z$ was measured far below the coil-globule crossover temperature as shown in Fig. 9. Since the time evolution of $\langle M \rangle_w$ calculated due to Eq. (17) is in good agreement with the observed one of Eq. (8) in the functional form and in the scaled form, the size distribution of Eq. (17) is likely to be appropriate for the present aggregation process. It is necessary to examine the scattering functions $\langle P(x) \rangle_z$ more closely. In the previous study, we calculated $\langle P(x) \rangle_z$ at different concentrations and times [$c \times 10^{-4} \text{ g/cm}^3$, $t(\text{min})$] as (1.30, 690), (2.66, 240), (4.04, 150), and (5.37, 90) with Eq. (14). By using Eq. (20) with $p = 0.138$ and $q = 0.71$, we recalculated $\langle P(x) \rangle_z$ at the same time and concentration and obtained a composite curve, which was 5% smaller than the previous one at $x^2 = 15$: the use of Eq. (20) resulted in a slightly larger disagreement. The ratio of observed and calculated values of $\langle P(x) \rangle_z$ at $x^2 = 15$ is 1.36 for $m = 2.35 \times 10^6$ and 1.49 for $m = 4.4 \times 10^6$. It should be noted that $\langle P(x) \rangle_z$ was calculated at different values of polydispersity of cluster size. In polymer characterization, the polydispersity is expressed with $\langle M \rangle_w / \langle M \rangle_n$, which is given by $\exp(Bct/m)$ in the present case. $\langle P(x) \rangle_z$ was found to be calculated at $\langle M \rangle_w / \langle M \rangle_n = 3.6, 4.9, 5.4,$ and 10.6 for $m = 2.35 \times 10^6$; and $2.7, 3.5, 4.5,$ and 6.0 for $m = 4.4 \times 10^6$ in the order of increasing time. Thus, the better agreement between the calculated and observed values of $\langle P(x) \rangle_z$ is obtained for the larger polydispersity for $m = 2.35 \times 10^6$. This indicates that the discrepancy in $\langle P(x) \rangle_z$ at large x^2 may stem from a structure of the cluster rather than from the size distribution given by Eq. (17). The cluster of polymer chains cannot be correctly represented by a spherical particle of uniform density.

It is interesting to visualize the time evolution of the size distribution given by Eq. (17). Figure 12 shows $N_1, N_2, N_3,$ and $\langle M \rangle_w / M(0)$ as a function of ct for $m = 4.4 \times 10^6$, where N_i is normalized as $\sum k N_k = 1$. At large ct , $N_1, N_2,$ and N_3 become very small and consequently, $\sum k N_k = 1$ may be contributed from numerous terms at large k . Thus, with increasing ct , the size distribution N_k becomes flatter with the tail extended to larger k . We calculated the ratio $\sum k^2 N_k / e^{gct}$, which is unity when the summation is taken from $k = 1$ to infinity. The ratios were calculated to be 1.000, 0.902, and 0.376 for $ct = 0.1, 0.2,$ and 0.3 , respectively, when the summation was taken from $k = 1$ to 50. At $ct = 0.3$ the contribution from terms for $k \geq 50$ to $\langle M \rangle_w$ exceeds 60%. This trend may be more remarkable in the calculation of the z -averaged square radius $\langle R^2 \rangle_z$.

Aggregations of colloidal particles have been studied in two different regimes, i.e., the fast aggregation process due to diffusion-limited cluster aggregation (DLCA) and the slow aggregation process due to reaction-limited cluster aggregation (RLCA) [10]. The two aggregation processes have been distinguished by the structure of the cluster and the time evolution of the cluster size distribution [11–15]. DLCA is represented by Eq. (11) with the collision kernel $K_{ij} = 8\pi DR$, where D and R are the diffusion constant and radius of a monomer, respectively [5]. For the initial condi-

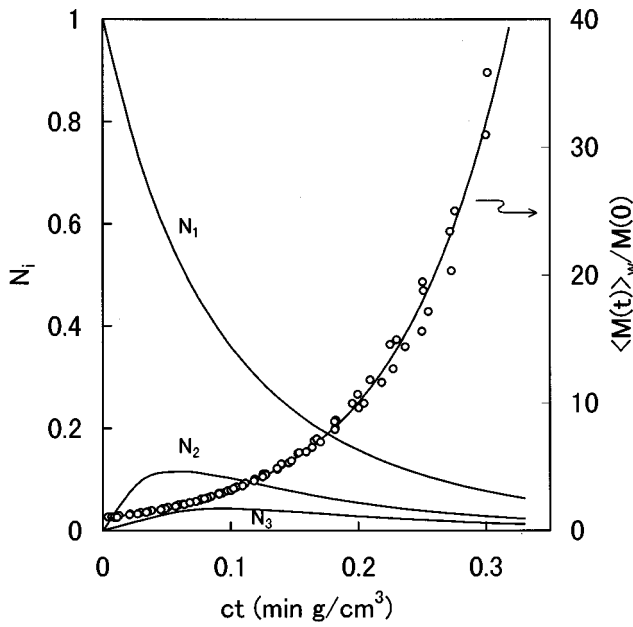


FIG. 12. Cluster size distribution as a function of ct . N_1 , N_2 , and N_3 are calculated by Eq. (17) with $g = 11.6$ and normalized by $\sum_k N_k = 1$. Data points represent the weight-average number of chains in a cluster obtained for $m = 4.4 \times 10^6$.

tion with monomers alone, Eq. (12) gives $\langle M \rangle_n = m(1 + 4\pi DRNt)$ and

$$\langle M \rangle_w = m(1 + 8\pi DRNt), \quad (22)$$

where $1/(8\pi DRN)$ is a characteristic time and expressed to be $3\eta/4kTN$ with the Stokes-Einstein relation $D = kT/(6\pi\eta R)$. Here, η is the viscosity coefficient and has been measured to be $\eta = 7.53 \times 10^{-4}$ Pa s for isoamyl acetate at 30.0°C . For the present solution with $c = 1.414 \times 10^{-4}$ g/cm³, the characteristic time is calculated to be 7.0×10^{-3} s, while the observed characteristic time is obtained from Eq. (8) as $1/gc = 610$ min. The ratio of the observed and calculated characteristic times is estimated as 5×10^6 . Thus, on account of the time scale and the form of the exponential growth, the observed aggregation process of the polymer chains cannot be compared with DLCA but with RLCA [10–15].

The Smoluchowski equation with the collision kernel $K_{ij} = B(i+j)$ gives Eq. (13): the rate $g = 2B/m$ of the aggregation decreases inversely proportional to the molecular weight of the polymer chain. Since we obtained $g = 52.2$ and 11.6 for $m = 2.35 \times 10^6$ and 4.4×10^6 , respectively, the observed rate decreases with the increasing m much faster than the prediction $g = 2B/m$. This implies that the coefficient B depends on the molecular weight of PMMA. In a previous study, we were able to measure the chain collapse processes for $m \times 10^{-6} = 8.4$ and 12.2 for long time periods of 1500 min and 9540 min after quench, respectively [2]. In the measurements, additional light scattering due to phase separation was negligibly small and the solutions appeared to be stable for the time period. Thus, very small values of g are expected for these high molecular weights. The slow collapse of the

polymer chain may be parallel behavior to the slow aggregation of polymer chains, because both the processes may be dominated by a specific reaction between segments of the polymer chain. The reaction may be the same regardless of whether the segments belong to a same chain or different chains.

Chu, Ying, and Grosberg carried out dynamic light-scattering measurements on a dilute solution of polystyrene in cyclohexane with $m = 8.12 \times 10^6$ and $c = 8.7 \times 10^{-6}$ g/cm³ and observed a single-chain collapse process for a time period of about 10 min after the quench of the solution [19]. For this solution the characteristic time is calculated as 0.2 s by Eq. (22) and the ratio of the observed and calculated characteristic times may be estimated as 10^3 , which is much smaller than the present ratio 10^6 . To explain the observed slow aggregation process for the polystyrene solution, Chuang, Grosberg and Tanaka performed a molecular dynamics simulation for a topological repulsive force acting between two approaching polymer globules [20]. According to the simulation, the entanglement force operational on the prereptational time scale was sufficient to explain the observed slow-down aggregation. On the other hand, the largely different ratios of characteristic times obtained by us and Chu Ying, and Grosberg suggest that the aggregation rate in a dilute polymer solution depends strongly on a specific nature of the solution. To elucidate the slow aggregation process it is important to distinguish the contributions from the specific nature of the solution and that from the universal nature of the chain entanglement, though the origin of the specific nature is not clear. The observed molecular weight dependence of the coefficient B may not be explained by the specificity of the polymer solution but by the entanglement force demonstrated by Chuang, Grosberg, and Tanaka.

In recent theoretical studies on polymer chain clusters below the θ -temperature [21,22], the radius and stability of the cluster were analyzed as a function of the two-body excluded volume parameter z , the three-body parameter, and the number k of chains in a cluster. The radii calculated for clusters of $k = 2, 3, 5,$ and 10 were represented graphically, and asymptotic behavior of the radius at large $-z$ and large k was conjectured. The calculation predicted the form of Eq. (14) with $D = 3$ at large $-z$ as expected for a compact globular cluster. A_k^3 s for clusters at large k were represented by a power law with the exponent $-2/3$, while in the present study, A_k in the whole range of k is expressed by Eq. (20). A small cluster such as those below $k = 10$ was predicted to have a smaller radius of gyration than a single polymer chain in a narrow temperature range between the stability temperature and chain collapse temperature. In Fig. 9, this temperature region may be located between the cloud point curve and the horizontal line extended to a higher concentration. Below the chain collapse temperature, the segment density of a single polymer chain was estimated to be as large as the critical nucleus for phase separation; the free energy barrier to the onset of the chain aggregation might vanish in the two-phase region near the dilute branch of the phase diagram. In the present cloud-point measurements that were carried out near the coil-globule crossover temperature, scattered intensity was observed to increase with a long lag time

after quench as mentioned in the experimental section. On the other hand, in the cluster aggregation experiments made at far below the cloud-point temperature, scattered intensity was observed to increase immediately after quench into the globule region. Furthermore, Figs. 2, 3, and 5 show that the cluster grows continuously from the size of a single polymer chain. The smooth cluster growth at small t is not indicative of a nucleation process with the free energy barrier but seems to suggest a phase separation near a spinodal. An exploration

of the spinodal in the present system is interesting but seems to be very difficult experimentally.

ACKNOWLEDGMENT

This work was supported by a Grant-in-Aid for Scientific Research (Contract No. 10640377) from the Ministry of Education, Science, Sports, and Culture of Japan.

-
- [1] M. Nakata and T. Nakagawa, *Phys. Rev. E* **56**, 3338 (1997).
[2] M. Nakata and T. Nakagawa, *J. Chem. Phys.* **110**, 2703 (1999).
[3] M. Nakata, T. Nakagawa, Y. Nakamura, and S. Wakatsuki, *J. Chem. Phys.* **110**, 2711 (1999).
[4] J. Turkevich and H. H. Hubbell, *J. Am. Ceram. Soc.* **73**, 1 (1951).
[5] M. von Smoluchowski, *Z. Phys. Chem., Stoechiom. Verwandtschaftsl.* **92**, 129 (1917); *Phys. Z.* **17**, 585 (1916).
[6] R. M. Ziff, in *Kinetics of Aggregation and Gelation*, edited by F. Family and D. P. Landau (North-Holland, Amsterdam, 1984).
[7] R. J. Cohen and G. B. Benedek, *J. Phys. Chem.* **86**, 3696 (1982).
[8] M. Nakata and K. Kawate, *Phys. Rev. Lett.* **68**, 2176 (1992).
[9] H. Sato, N. Kuwahara, and K. Kubota, *Phys. Rev. E* **50**, R1752 (1994).
[10] T. Vicsek, *Fractal Growth Phenomena* (World Scientific, Singapore, 1989).
[11] D. A. Weitz, J. S. Huang, M. Y. Lin, and J. Sung, *Phys. Rev. Lett.* **54**, 1416 (1985).
[12] R. C. Ball, D. A. Weitz, T. A. Witten, and F. Leyvraz, *Phys. Rev. Lett.* **58**, 274 (1987).
[13] J. E. Martin, *Phys. Rev. A* **36**, 3415 (1987).
[14] M. Y. Lin, H. M. Lindsay, D. A. Weitz, R. C. Ball, R. Klein, and P. Meakin, *Nature (London)* **339**, 360 (1989).
[15] J. E. Martin, J. P. Wilcoxon, D. Schaefer, and J. Odinek, *Phys. Rev. A* **41**, 4379 (1990).
[16] J. P. Kratochvíl, G. J. Deželić, M. Kerker, and E. Matijević, *J. Polym. Sci.* **57**, 59 (1962).
[17] P. Kratochvíl, *Classical Light Scattering from Polymer Solution* (Elsevier, Amsterdam, 1987).
[18] M. Kerker, *The Scattering of Light and Other Electromagnetic Radiation* (Academic, New York, 1969).
[19] B. Chu, Q. Ying, and A. Yu. Grosberg, *Macromolecules* **28**, 180 (1995).
[20] J. Chuang, A. Yu. Grosberg, and T. Tanaka, *J. Chem. Phys.* **112**, 6434 (2000).
[21] G. Raos and G. Allegra, *Macromolecules* **29**, 6663 (1996).
[22] G. Raos and G. Allegra, *J. Chem. Phys.* **107**, 6479 (1997).